GeoMin3D: Advances in electrical and EM data modelling and inversion

Guy Marquis, Ali Mohand-Said, Alessandro Vinciguerra, Jean-Francois Girard, University of Strasbourg - ITES
Grant Harrisson, Orano Canada Inc.
Elodie Williard, Orano Mining

gmarquis@unistra.fr

The GeoMin3D project

GeoMin3D is joint industry-academic program that aims to bring a paradigm shift in unconformity-related uranium deposit exploration by leveraging our scientific and technological findings into innovative exploration technologies. The program aims to improve data acquisition and modeling processes, to bring out new scientific and technical concepts to favor a better understanding of the deposits and their targeting, to improve the use and usability of variable datasets and promote reconciliation between geophysical and geological information. Dr Julien Mercadier from Nancy presents an overview of the GeoMin3D project in an oral presentation Tuesday at 1050. This poster focuses on the geophysical developments of the project.

GeoMin3D partners are Laboratoire GeoRessources, Nancy, Institut Terre et Environnement de Strasbourg and Orano Mining. Funding for the project is provided by Orano and ANR (France's equivalent of NSERC).

Geophysics in the Athabasca

The Athabasca Basin is a world-class uranium mining province hosting high-grade high-tonnage deposits (Figure 1 Left). Uranium mineralization is found at the unconformity (UC) where Proterozoic basin sediments overlie Archean to Paleoproterozoic metamorphic basement rocks. Deposits are also closely associated to steeply-dipping graphite-bearing faults and shear zones. Graphite-rich faults acted as hydrothermal fluids pathways. Fluid circulation led to clay alteration of hosting rock and uranium mineralization (Figure 1 Right).

Thus, the association of graphite-rich faults and alteration haloes correspond to a target for uranium exploration. Electrical resistivity of graphitic conductors is ranging from few $\Omega.m$ to few tens of $\Omega.m$ while basin sediments and basement rocks have resistivities ranging from 1000 $\Omega.m$ to 10000 $\Omega.m$. Alteration of hosting rocks decreases their resistivity (Figure 1D). Thus, geophysical methods sensitive to electrical resistivity are preferred to identify the geological structures associated to uranium mineralization. When looking for uranium deposits in the Athabasca basin, Time-Domain Electromagnetic (TDEM) methods are used to locate graphitic faults, while Direct-Current Resistivity (DC) methods are used to identify alteration haloes (e.g. Nimeck and Koch, 2008).

Although TDEM and DC methods are sensitive to electrical resistivity, the signals measured do not carry the same information about the subsurface. TDEM and DC dataset are usually processed separately. Graphitic conductors' location and geometry are in practice well identified using plate-modelling software or an inversion algorithm. Signal from graphitic faults and alteration haloes are recorded in DC resistivity datasets. However, on inversion results, the footprint of graphitic faults overprints the signature from possible contrasts associated to alteration in the host-rocks.

Taking advantage of their specific sensitivity in a 2D joint inversion, we are expecting to constrain the extent of the graphitic conductors, allowing to model the resistivity contrast within sandstones and close to the unconformity, related to fluid flow and recorded in the signal of DC data (*cf. central panel*).

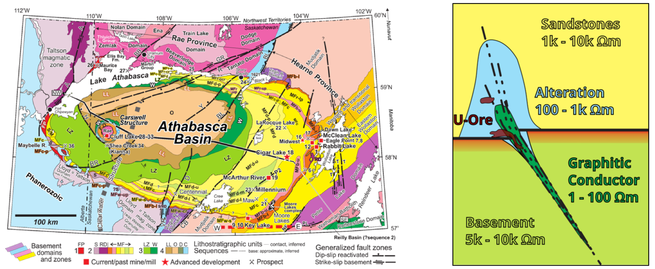

Figure 1: Left: Major structures of Athabasca Basin, Right: Simplified Geological Model of Athabasca U-deposits (Modified from Jefferson et al., 2007).

References

[1] Cockett R., Kang S., Heagy L.J., Pidlisecky A., and Oldenburg D.W. Simpeg: An open source framework for simulation and gradient based parameter estimation in geophysical applications. *Computer and Geosciences*, 2015.

[2] Conn A.R., Gould N.I.M., and Toint P.L. *Trust Region Methods*. Society of Industrial and Applied Mathematics, 2000.

[3] Nimeck G. and Koch R. A progressive geophysical exploration strategy at the shea creek uranium deposit. *The Leading Edge*, 2008.

[4] Nocedal J. and Wright S.J. *Numerical Optimization*. Springer, 2006.

[5] C.J.F. ter Braak and Vrugt J.A. Differential evolution markov chain with snooker updater and fewer chains. *Statistics and Computing*, 2008.

[6] A. Raiche, Sugeng F., and Wilson G. Practical 3d em inversion – the p223f software suite. *ASEG Extended Abstracts*, 2007.

Inversion of moving-loop TEM and DC data using trust-regions

(PhD thesis of Ali Mohand Said, amohandsaid@unistra.fr)

Joint Inversion methodology

Our joint inversion methodology finds a single resistivity model minimizing the square of the L2-norm of weighted TDEM and DC data discrepancies. Forward modeling of TDEM and DC responses were done using SimPEG codes (Cockett et al. 2015; Heagy et al. 2018), which also allows to compute the sensitivity matrices using the adjoint-state method. Modeling of Pole-Dipole survey was made in 2D, while Moving Loop TDEM modeling was made in 3D by extending a model defined on a 2D section.

Solving DC and TDEM forward problems is requiring different discretizations. To obtain a single resistivity model, inverse problem must be solved on a separate grid. The connection between the inversion grid and DC and TDEM discretization was made using Non-Uniform Rational B-Splines (NURBS, Bingol and Krishnamurthy 2019) interpolators B_{em} and B_{dc} (eq. 1 and 2). Thus, we invert NURBS coefficients (m) instead of resistivity:

$$m_{em} = B_{em}\, m \; [eq.1] \quad m_{dc} = B_{dc}\, m \; [eq.2]$$

The sensitivity matrices (Jacobians) J_{em} and J_{dc} are obtained on the grids of forward modeling. Using the chain rule of derivatives, it is easy to get partial derivatives with respect to the NURBS coefficients $J_{NURBS_{em}}$ and $J_{NURBS_{dc}}$ (eq. 3 and 4):

$$J_{NURBS_{em}} = J_{em} B_{em} \; [eq.3] \quad J_{NURBS_{dc}} = J_{dc} B_{dc} \; [eq.4]$$

A Gauss-Newton Trust-Region algorithm (Conn et al. 2000, Nocedal and Wright 2006) was used [eq. 6]. The effective sensitivity matrix of NURBS coefficients (J) is a concatenation of weighted (W_{em}, W_{dc}) interpolated sensitivities [eq. 5] which leads to a weighted summation of TDEM and DC gradients and Gauss-Newton approximations of Hessian matrices.

$$J = \begin{bmatrix} W_{em} J_{NURBS_{em}} \\ W_{dc} J_{NURBS_{dc}} \end{bmatrix} \; [eq.5] \quad (J^T J + \lambda I)\Delta m = -J^T (d_{calc} - d_{obs}) \; [eq.6]$$

Area of interest and surveys configuration

The area of interest is in the eastern part of the Athabasca basin. A Time Domain EM (TDEM) Moving Loop ground survey was acquired in 2015. Measurements of magnetic flux were made over several lines oriented N-S, perpendicular to previously identified magnetic and conductive trends. For our work we selected vertical component of magnetic flux data over 15 time gates ranging from 0.1 ms to 2.0 ms at 26 stations, along a single line, with a spacing of 200m (Figure 2 top). Receivers were located 800m to the north of the 400m-edge square loop transmitter. Data from a Pole-Dipole survey acquired in 2016 on the same area were available. We selected apparent resistivity data from a line coincident with the Moving Loop measurements (Figure 2 bottom). The dipole length is 100m, and the current injections were made every 100m. Measurements with a geometric factor greater than 100000 were discarded. The total length of the DC line is 5600m

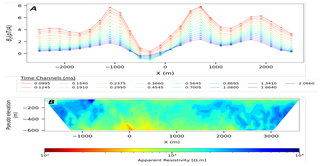

Figure 2: Field data acquired from Athabasca Basin: Moving Loop TDEM data (A); Pole-Dipole DC Resistivity data (B).

Field data inversion

DC standalone inversion fits well the DC (Figure 4A) data but not the TDEM data (Figure 5A). And reciprocally for the TDEM standalone inversion (Figures 4B and 5B). Joint inversion allows to fit both datasets (Figure 4C and 5C). Looking at the resistivity models, the TDEM inversion (Figure 3B) is displaying several steeply-dipping conductive structures at depth between 400 m and 500 m. The standalone DC inversion (Figure 3A) is showing an extend conductive object at the same range of depth. But we cannot assess the occurrence of alteration. The resistivity model obtained with the joint inversion (Figure 8C) is showing the conductive plates already identified on the TDEM inversion. But we can also see a horizontal layers of 500 $\Omega.m$ to 1000 $\Omega.m$ overlying the top of the plate. A lower resistivity at the unconformity could be expected as it constitutes a pathway for hydrothermal fluids. Moreover, the first few meters a the top of the basement often show paleo-weathering markers.

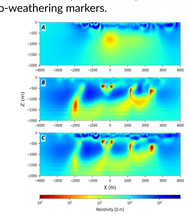

Figure 3: Field data inversion resistivity models: Standalone DC inversion (A); Standalone TDEM inversion (B); Joint inversion (C).

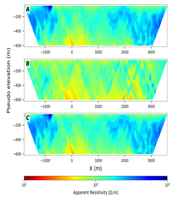

Figure 4: Field data inversion DC predicted data: Calculated on model from DC inversion (A); Calculated on model from EM inversion inversion (B); Calculated on model from Joint inversion (C).

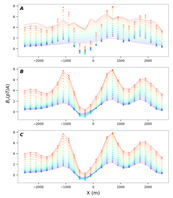

Figure 5: Field data inversion TDEM predicted data: Calculated on model from DC inversion (A); Calculated on model from EM inversion inversion (B); Calculated on model from Joint inversion (C).

Estimation of conductive thin plates parameters through a Bayesian approach

(Postdoc of Alessandro Vinciguerra, avinciguerra@unistra.fr)

Inversion algorithm

The Bayesian inversion strategy allows to solve the inverse problem taking in account the prior information on the subsurface and assessing the uncertainty in terms of posterior probability density function (pdf). In this work, we implemented the Differential Evolution Markov Chain (ter Braak et al. 2008), a multi-chain algorithm that guarantees a faster convergence than the basic random walk algorithm.

Let the model vector m being defined by:

$$m = [\rho_b, \rho_s, \rho_p, \phi x_{pos}, z] \quad [eq.7]$$

where ρ_b, ρ_s and ρ_p are the resistivity of the bedrock, layer and plate, respectively. ϕ is the dip of the plate, x is the position of the top along the profile and z the depth of the top. The algorithm employs at least three chains composing the population that evolve during generation through the updating relation:

$$m_{i+1}^{a} = m_i^{a} + \gamma(m_i^{b} - m_i^{c}) + e \quad [eq.8]$$

where a, b, c are the indices of the chains, i is the iteration index, γ is a user-defined scalar and e is a random perturbation drawn from $N(0, b)$ with b small. At each iteration the model m of each chain has the following acceptance probability:

$$\alpha = min\left(1, \frac{like(m_{upd})\, p(m_{upd})}{like(m_{curr})\, p(m_{curr})}\right) \quad [eq.9]$$

where $like$ is the likelihood function, m_{upd} is the model updated through [], m_{curr} the current model and $p(...)$ is the prior probability associated to the considered model (current or updated). The model is accepted or rejected following the Metropolis-Hastings rule: accepted if $\alpha > u$, rejected if $\alpha < u$ with $u \in [0, 1]$.

Application to a Moving-Loop TDEM synthetic case

We computed the response using *Leroi* algorithm (Raiche et al. 2007) for a Moving-Loop TDEM survey with a TX-RX offset of 800 m over a two-layer model containing a subvertical plate with its top at the layer interface (Figure 6 right).

The DEMC is set employing three Markov chains to sample the pdf defined by the six parameters of Equation 7. Figure 6 (left) suggests that after about 500 iterations, each chain reaches the stationary regimes where the DEMC samples the posterior probability density function. Moreover, the data computed employing the mean model is able to fit the synthetic data (Figure 6 right).

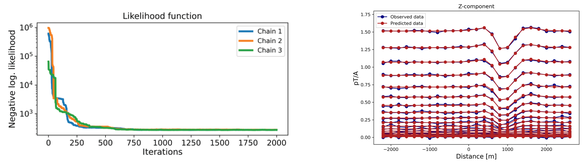

Figure 6: Left: Negative log likelihood of the three chains, Right: The predicted data (in red) is able to reconstruct the observed one, especially at early times.)

Starting from marginal prior distributions (Figure 7), the DEMC is able to sample the posterior pdf from which the mean and the standard deviation is computed. All the parameters are well-recovered with an acceptable standard deviation.

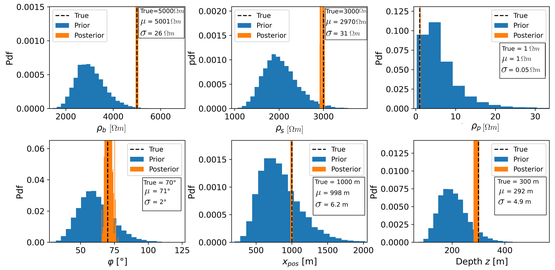

Figure 7: Marginal distribution of the model parameters. In blue the prior, in orange the posterior and the dashed line represents the true value.